Characterization of Higher-Order Structure of Poly(ethylene-2,6-naphthalate) Treated with Supercritical Carbon Dioxide

Shigeo Asai,* Yuuki Shimada, Yoichi Tominaga, and Masao Sumita

Department of Chemistry and Materials Science, Tokyo Institute of Technology, Ookayama, Tokyo 152-8552, Japan

Received February 22, 2005; Revised Manuscript Received June 6, 2005

ABSTRACT: We have prepared poly(ethylene-2,6-naphthalate) (PEN) films having higher-order structure with fine crystallites using a supercritical carbon dioxide ($scCO_2$) treatment technique at a relatively low-temperature range, from 110 to 170 °C. After the $scCO_2$ treatment, the glass transition temperature T_g decreased by more than 50 °C, and the PEN films were crystallized. Long-term change in the FT-IR absorbance intensity at 2335 cm^{-1} (C═O) was in good agreement with the change in T_g. The large decrease in T_g was attributed to the sorption of the CO_2 molecules into the PEN film. Moreover, the increase in the treatment pressure increased the amount of absorbed CO_2 and reduced T_g, which can promote crystallization. The higher-order structure, long period, lamella, and interface thickness of the crystallized PEN films were calculated from the one-dimensional correlation function by SAXS. These parameters were all linearly related to the treatment temperature. The crystallite size obtained from the Scherrer equation decreased with decreasing treatment temperature. It is suggested that the higher-order structure of PEN is decided only by the treatment temperature and that the $scCO_2$ treatment promotes the creation of the nuclei in the amorphous state at low temperatures, following the formation of fine crystallites.

Introduction

Poly(ethylene 2,6-naphthalate) (PEN) is a semicrystalline engineering plastic with commercial application. It can be used for high-temperature applications such as containers, hollow bodies, and bottles. The naphthalene ring provides greater rigidity to the polymer backbone than does the benzene ring in poly(ethylene terephthalate) (PET), raising the glass transition temperature and melting point and enhancing mechanical properties such as the tensile modulus and creep resistance. The crystal structure of PEN has already been studied by many research groups.[1−6] Crystallization from the unoriented glass or from the melt state below 200 °C leads to a one-chain triclinic α-form (a = 0.651 nm, b = 0.575 nm, c = 1.32 nm, α = 81.33°, β = 144°, γ = 100°, density: 1.407 g/m^3).[2,4] The triclinic β-form of PEN crystal is obtained by melt-crystallization at a lower temperature than the melting point,[2] by drawing,[7−9] high-pressure treatment,[10−12] solvent induced,[13] flow induced,[14] and shearing.[15] Since the crystalline form of PEN varies with the conditions, it is necessary to characterize the detailed crystalline and higher-order structure.

Supercritical fluid (SCF) shows extraordinary physicochemical properties above its critical temperature and pressure, T_c and P_c. SCF exhibits superior mass-transfer characteristics than the liquid, including lower viscosity and higher diffusivity.[16] SCF also provides considerable control over the thermodynamic and transport characteristics with variations in pressure and temperature. In particular, the properties of supercritical carbon dioxide ($scCO_2$) have attracted much attention in the preparation of advanced materials because of its nontoxicity, its nonflammability, and its inexpensiveness.[16−18] Carbon dioxide has a relatively low critical point (T_c = 31 °C, P_c = 7.4 MPa), and $scCO_2$ is designated environmentally as a "benign solvent". Its unique properties have great potential in polymer science, in polymer synthesis,[19] and in polymer processing such as microcellular forms, particles, polymer blends, crystallization, dyeing, and coatings.[18]

Swelling of certain polymers due to sorption of small molecules such as organic solvents reduces the T_g of the amorphous phase following crystallization. Use of CO_2 as a solvent also leads to a decrease in T_g, since CO_2 molecules can easily absorb into polymers under pressurized conditions. For instance, Handa et al. found that the high-pressure DSC system led to a decrease of more than 40 °C in the T_g of polystyrene (PS).[20] Several groups have reported that CO_2 is a good crystallizable agent for some polymers including polyethylene,[21] syndiotactic PS,[22] poly(vinylidene floride),[23] PET,[24] polycarbonate,[25] poly(phenylene sulfide),[26] and poly(ether ether ketone).[27] Sorption of the CO_2 molecules has a plasticizing effect on polymers.[28−30] During the processing, some polymers having electron-donating groups such as carbonyls undergo specific interactions with absorbed CO_2, probably of Lewis acid−base nature.[31,32] It is therefore possible to reduce T_g and induce crystallization in CO_2 even for polymers which have higher T_g and crystallization temperatures. In this study we have treated amorphous PEN films with $scCO_2$ under various conditions of temperature and pressure and have determined the effect of CO_2 on the crystallization behavior and higher-order structure using small-angle X-ray scattering (SAXS). The detailed higher-order structure of PEN is clearly revealed.

Experimental Section

Sample Preparations. The PEN film used in this study, of thickness 83 μm, was supplied by Teijin Co. The original film was confirmed by DSC and WAXD measurements to be

* Corresponding author: e-mail sasai@o.cc.titech.ac.jp; Tel +81-3-5734-2432; Fax +81-3-5734-2876.

10.1021/ma050373q CCC: $30.25
Published on Web 06/30/2005

completely amorphous. Supercritical CO_2 treatment films were prepared using a $scCO_2$ extraction system (JASCO Co., Ltd.) consisting of a delivery pump (SCF-Get), an automatic back-pressure regulator (SCF-Bpg), and a heater. A high-pressure reactor (maximum 35 MPa, 400 °C) made of SUS−Ni alloy (Hastelloy) was constructed from a retainer and a vessel (80 mL) with an Au-coated copper seal. The amorphous PEN film was introduced into the vessel and kept at a constant temperature. Liquid CO_2 was pumped into the reactor from the delivery pump at a rate of 10 mL/min, and the vessel was maintained at a constant pressure with a CO_2 flow rate of 2 mL/min. The treatment temperature, pressure, and time varied between 40 and 170 °C, 10 and 20 MPa, and 15 and 1440 min. After treatment for a predetermined time, the vessel was quenched in iced water, following the film was taken out and dried in a vacuum at 30 °C for at least 2 days.

Cold-crystallized film was prepared from the amorphous PEN film treated at a constant temperature using a FP80HT hot stage (Mettler Toledo) followed by quenching in iced water.

Measurements. Differential scanning calorimetry (DSC) measurements were carried out using a DSC-50 (Shimadzu Co.) in the temperature range from −10 to 300 °C at a heating rate of 20 °C/min under a nitrogen gas atmosphere.

Fourier transformed infrared (FT-IR) spectra were measured using a FT/IR-620 system (JASCO Co., Ltd.) consisting of a MICRO-20 and a ATR-JC-Z unit with a resolution of 2 cm^{-1}.

Wide-angle X-ray diffraction (WAXD) measurements were carried out using a RINT-2000 system (Rigaku Co.) with Cu Kα radiation ($\lambda = 0.154\ 18$ nm) operating at 40 kV and 40 mA. The system was equipped with a graphite monochromator and a scintillation counter in the diffraction angle range between 3° and 60°. The degree of crystallinity χ_c for each film was determined according to the equation

$$\chi_c = \frac{\int_{2\theta_1}^{2\theta_2} I_c(2\theta)\, d(2\theta)}{\int_{2\theta_1}^{2\theta_2} I(2\theta)\, d(2\theta)} \tag{1}$$

where the values of $2\theta_1$ and $2\theta_2$ used in this study are 7° and 35°. The average crystallite size (D_{hkl} nm) for the direction normal to the (hkl) plane was determined from the Scherrer equation

$$\Delta(2\theta) = \frac{0.94\lambda}{D_{hkl}\cos\theta} \tag{2}$$

where $\Delta(2\theta)$ is the half-width of the diffraction peak at 2θ. This equation supposes that the crystals are perfect.

Small-angle X-ray scattering (SAXS) measurements were carried out using a RU-200 system (Rigaku Co.) with Ni filtered Cu Kα radiation operating at 50 kV and 180 mA and a scintillation counter in the scattering angle between 0.08° and 2.5°. For collimation, the first slit was 0.08 mm, the second slit was 0.06 mm, and the receiving slit was 0.1 mm; the scattering slit was 0.25 mm wide. The higher-order structure consisting of crystalline and amorphous regions can be characterized as a three-phase model (pseudo-two-phase model consists of lamella, amorphous, and interface between lamella and amorphous). The long period (the sum of lamella, amorphous, and interface thickness) was estimated from the one-dimensional correlation function, $\gamma_1(x)$, defined as[33]

$$\gamma_1(x) = \frac{\int_0^\infty s\tilde{I}(s)[J_0(2\pi xs) - 2\pi xsJ_1(2\pi xs)]\, ds}{\int_0^\infty s\tilde{I}(s)\, ds} \tag{3}$$

where J_0 and J_1 are the zero- and first-order Bessel functions, x is the correlation length, s is the absolute value of the scattering vector ($= 2\pi \sin\theta/\lambda$), and $\tilde{I}(s)$ is the slit-smeared intensity after removing the air scattering and the scattering background corresponding to electron density fluctuations within the phases.

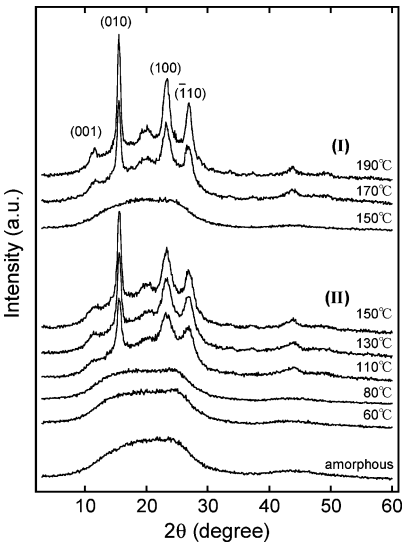

Figure 1. WAXD patterns in (I) cold-crystallized and (II) $scCO_2$-treated PEN films at 20 MPa for 90 min with different treatment temperatures.

The interface thickness between the crystal (or lamella) phase and the amorphous phase was estimated from the diffuse phase boundary thickness, which can be determined using the SAXS method outlined by Ruland.[34] According to the infinite slit collimation, the asymptotic scattering intensity, assuming a sigmoidal-gradient model, can be expressed in the empirical form[35]

$$\lim_{s\to\infty} \tilde{I}(s) = \frac{K}{s^3}\exp[-38(\sigma s)^{1.81}] \tag{4}$$

where K is the Polod law constant and σ is the standard deviation of the Gaussian smoothing function used to generate the sigmoidal diffuse phase boundary gradient and is a measure of the thickness of the boundary. The value of σ is obtained from the gradient of the plot of $\ln\{s^3\tilde{I}(s)\}$ vs $s^{1.81}$:

$$\sigma = \left(\frac{-\text{slope}}{38}\right)^{1/1.81} \tag{5}$$

This standard deviation can be given a more physical interpretation by comparison with the linear gradient model. The width of the linear gradient E is approximately related to the sigmoidal gradient by the expression:

$$E \cong \sqrt{12}\sigma \tag{6}$$

Results and Discussion

Crystallization Behavior of $scCO_2$-Treated PEN. To investigate the effect of the treatment temperature on crystallization behavior, amorphous PEN films were treated with $scCO_2$ for 90 min at various temperatures under a constant pressure of 20 MPa. As a reference, cold-crystallized PEN films were also prepared at various temperatures for 90 min under air. Figure 1 summarizes the change of WAXD patterns in the PEN films treated at temperatures from 60 to 190 °C. The WAXD patterns (I) of PEN films which have been crystallized at temperatures between 170 and 190 °C exhibit diffraction peaks, whereas the cold-crystallized film at 150 °C possesses an amorphous halo without any diffraction peaks, like an amorphous pattern. It has been reported that cold-crystallized films are characterized as the α-form by their (001), (010), (100), and ($\bar{1}$10) reflections.[2] Zahamman et al. found that the crystal-

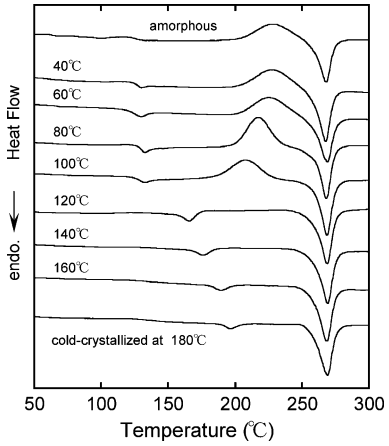

Figure 2. DSC curves of amorphous, cold-crystallized at 180 °C, and $scCO_2$-treated PEN films with different treatment temperatures.

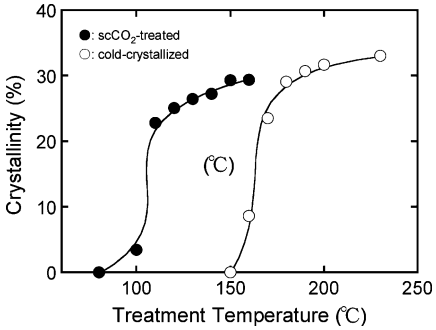

Figure 3. Treatment temperature dependence of crystallinity calculated from WAXD.

lization temperature of the α-form should be higher than 150 °C under air.[2] However, the patterns (II) of the $scCO_2$-treated films exhibit clear diffraction peaks attributed to the α-form although the treatment temperature is lower than 150 °C. The crystallization temperature may be reduced by the $scCO_2$ treatment, since crystallization of the $scCO_2$-treated PEN film at 110 °C has also been observed.

Figure 2 shows the DSC curves of the amorphous PEN films, that cold-crystallized at 180 °C, and that treated with $scCO_2$ at temperatures between 40 and 160 °C at a pressure of 20 MPa for 90 min. The $scCO_2$-treated films at 40 and 60 °C have almost identical curves to the amorphous film. The exothermic peaks of the treated films shift gradually to lower temperatures with increasing temperature between 40 and 100 °C. There is almost no difference in T_g between these films. However, the enthalpies of the exothermic and endothermic peaks corresponding to crystallization and melting have the same values; crystallization scarcely occurs with $scCO_2$ treatment up to 100 °C. The absence of an exothermic peak for the crystallized films at 120, 140, and 160 °C implies that these films have already been crystallized by the $scCO_2$ treatment before the DSC measurement. These films also have a small endothermic peak at a temperature ∼10 °C higher than the $scCO_2$ treatment temperature and below the melting point. This is probably due to the fusion of small and/or disordered crystallites which are often formed in semicrystalline polymers.

In Figure 3, the degrees of crystallinity calculated from eq 1 are plotted against the treatment temperatures for the $scCO_2$-treated and cold-crystallized films.

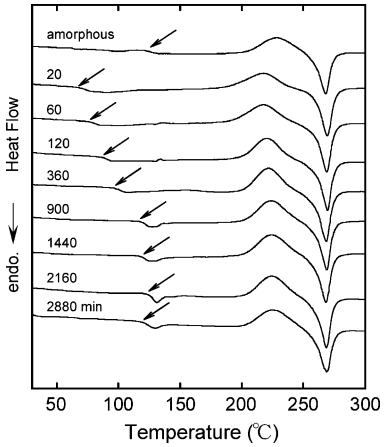

Figure 4. DSC curves of $scCO_2$-treated PEN films at 60 °C and 20 MPa for 90 min with different elapsed time.

The range of crystallization temperatures for the $scCO_2$-treated films is ∼50 °C lower than that for the cold-crystallized films. The temperature shift agrees with the decrease in T_g which was observed from the DSC curves, as seen in Figure 4. This indicates that the shift of the temperature range is due to sorption of CO_2 molecules into the sample film during the $scCO_2$ treatment. In a comparison of the two films which were crystallized at 160 °C, the $scCO_2$-treated film should exhibit higher crystallinity than the cold-crystallized film. There is an acceleration of the crystallization due to the treatment. In general, the rate of crystallization depends on the crystallization temperature, and the temperature giving the maximum crystallization rate T_{max} is approximately midway between T_g and the equilibrium melting point T_m^0. Between T_g and T_{max} is the *crystal-growth region* in which the crystallization rate should be controlled by the crystal growth rate. The temperature interval between T_{max} and $T_m{}^0$ is called the *nucleation-control region*, in which the crystallization rate should be controlled by the nucleus growth rate. In this study the crystallization rate is controlled by the crystal growth rate, since the $scCO_2$ treatment temperatures are below T_{max}. Enhancement by CO_2 of the crystallization at 160 °C is therefore probably due to the increase in the crystal growth rate caused by the reduction in T_g and increasing molecular mobility.

Continuous Change in T_g. Figure 4 shows changes in the DSC curves for PEN films treated with $scCO_2$ at 60 °C under a pressure of 20 MPa for 90 min as a function of elapsed time. The numerals in this figure denote the time elapsed after the treatment. The $scCO_2$-treated PEN film was used without the drying process. It is confirmed that the film possesses only the amorphous phase. The T_g of untreated amorphous film is ∼125 °C, whereas the T_g of the $scCO_2$ treatment film after 20 min is ∼70 °C. The T_g value after the $scCO_2$ treatment increases with increasing elapsed time and returns to its original level of ∼125 °C at times between 900 and 2880 min. It also seems that the treated film exhibits a small drop and gradual increase in the crystallization temperature (T_c) at the top of the peak. FT-IR measurement was therefore performed to confirm that the decrease in T_g and T_c is due to the sorption of CO_2. Figure 5a shows the FT-IR spectra of amorphous PEN film, $scCO_2$-treated film at 60 °C and 20 MPa and $scCO_2$-treated film at 120 °C and 20 MPa. The spectra of $scCO_2$-treated films were measured at 15 min after treatment. The absorbance was standardized with the

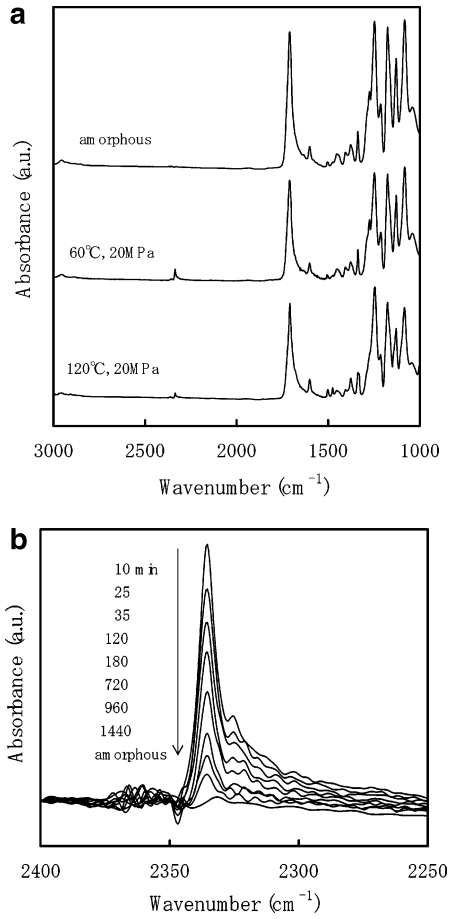

Figure 5. (a) FT-IR spectra of amorphous PEN film (top), $scCO_2$-treated film at 60 °C and 20 MPa (middle), and $scCO_2$-treated film at 120 °C and 20 MPa (bottom). The spectra of $scCO_2$-treated films were measured at 15 min after treatment. (b) Elapsed time dependence of FT-IR spectra at around 2335 cm^{-1} for $scCO_2$-treated PEN at 60 °C and 20 MPa.

absorbance of the naphthalene band at 1602 cm^{-1}. The band at around 2335 cm^{-1}, which is assigned to the symmetrical stretching vibration derived from the CO_2 molecules (C═O), was not observed for the amorphous film but was present for the $scCO_2$-treated films. This indicates that the CO_2 molecules remain in the film even after $scCO_2$ treatment. Moreover, the absorbance at the 2335 cm^{-1} band for the $scCO_2$-treated films at 60 °C, which is uncrystallized film, is clearly larger than that for the $scCO_2$-treated film at 120 °C, which is crystallized film. This suggests that CO_2 molecules in the supercritical state absorb preferentially into the amorphous phase rather than the crystalline phase. Figure 5b shows changes in the FT-IR spectra at around 2335 cm^{-1} for the PEN film treated with $scCO_2$ at 60 °C and 20 MPa as a function of elapsed time. Monotonic decrease in the C═O band was observed as a result of desorption of CO_2 after $scCO_2$ treatment. Figure 6a compares the elapsed time dependences of the C═O absorbance intensity at 2335 cm^{-1} and the T_g for a $scCO_2$-treated film at 60 °C and 20 MPa. The absorbance intensity based on the C═O vibration of absorbed CO_2 molecules decreases with increasing T_g. The linear relation can be confirmed in a plot of T_g and T_c vs C═O absorbance intensity as shown in Figure 6b. Under supercritical conditions, the excess CO_2 molecules that have absorbed into the film may cause on increase in free volume, following the decrease in T_g and T_c.

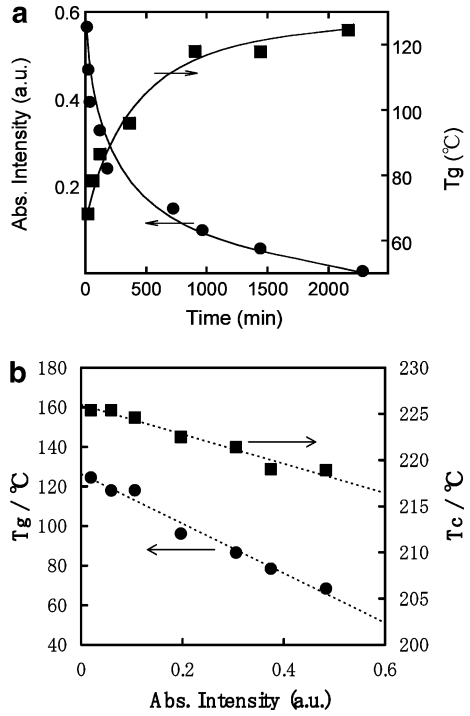

Figure 6. (a) Elapsed time dependence of FT-IR absorbance intensity at 2335 cm^{-1} and T_g for $scCO_2$-treated PEN at 60 °C and 20 MPa. (b) T_g and T_c vs absorbance intensity.

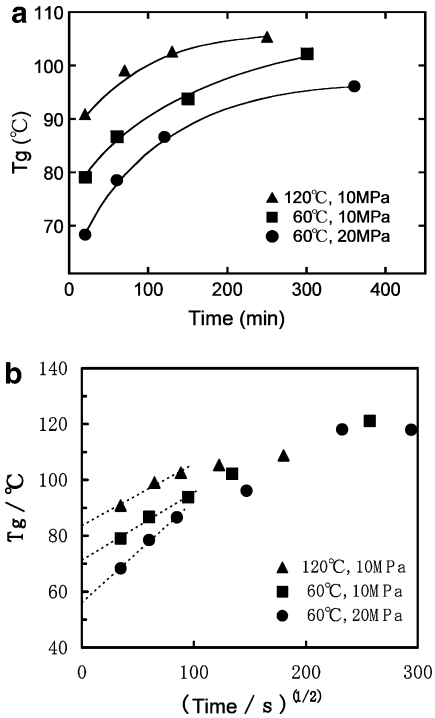

Figure 7. (a) Relation between T_g of $scCO_2$-treated PEN films and elapsed time (t) under different conditions. (b) T_g vs $t^{1/2}$ plot.

Effect of Treatment Pressure on T_g and Crystallization. The change in T_g for the $scCO_2$-treated PEN films is also influenced by the treatment conditions of temperature and pressure because these affect the CO_2 density. Figure 7a summarizes the relation between T_g for the crystallized PEN films and the elapsed time for differing conditions of temperature and pressure. The decrease in T_g for the PEN films which were crystallized at lower temperature and higher pressure is the largest

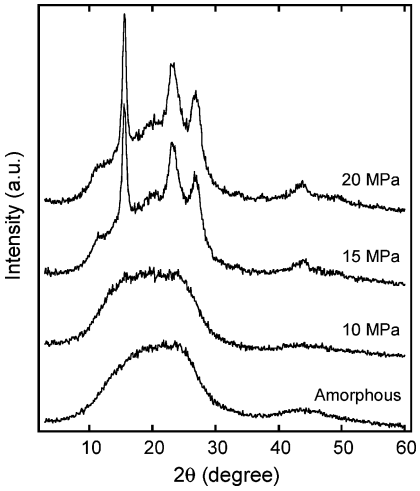

Figure 8. WAXD patterns of amorphous and $scCO_2$-treated PEN films crystallized at different CO_2 pressures.

(see data at 60 °C and 20 MPa). This indicates that the concentration of absorbed CO_2 molecules in the PEN films is larger under those conditions. In other words, the change in T_g was caused by the change in CO_2 solubility for the PEN film, which is related to the density of pure CO_2. The T_g value gradually increases with increasing time, but the value is much lower than the original T_g (~125 °C). This is because few CO_2 molecules remain in the treatment films after at least 300 min. The linear relation in the T_g vs C=O absorbance as shown in Figure 6b allows us to analyze the desorption kinetics presented in Figures 6a and 7a. Figure 7b shows the T_g vs $t^{1/2}$ plot in order to estimate the T_g under CO_2 exposure conditions by extrapolation of the T_g back to $t = 0$. The T_g's under the $scCO_2$ conditions of 120 °C/10 MPa, 60 °C/10 MPa, and 60 °C/20 MPa are roughly estimated as 84, 71, and 56, respectively. Moreover, the PEN films treated at various pressures have been prepared to characterize the effect of CO_2 conditions on the crystallization behavior. Figure 8 shows WAXD patterns of amorphous and crystallized PEN films treated at different CO_2 pressures. In this figure the crystallization temperature and time were chosen as 120 °C and 90 min. No diffraction peaks for a film crystallized at 10 MPa were observed, as for the amorphous pattern. In contract, the peaks in the films crystallized at 15 and 20 MPa are clearly observed. From the WAXD patterns, the crystallinity of the treatment film at 15 and 20 MPa films was calculated as 22.1 and 25.1%, respectively. From Figure 7a, there is a relatively small further decrease in T_g with increasing treatment pressure. Higher-pressure CO_2 treatment may increase the concentration of absorbed CO_2 molecules; the segment motion of the amorphous phase is probably enhanced, promoting crystallization.

Characterization of Higher-Order Structure by SAXS. Figure 9 summarizes the relations between higher-order structure, long period, lamella, and interface (including two interfaces between crystalline and amorphous phase) thickness and treatment temperatures for $scCO_2$-treated (110−160 °C, 20 MPa) and cold-crystallized (170−230 °C) PEN films. All films in this figure were treated for 90 min. The *c*-axis length (=1.32 nm) at the bottom of Figure 9 represents the repeat unit of the original PEN in the *c*-axis direction. This figure shows that the higher-order structure of all films developed gradually with increasing treatment temperature; the data seem to fall on a straight line despite the different treatment methods, $scCO_2$ treatment and cold crystallization. Moreover, the long period, lamella, and interface thickness of the $scCO_2$-treated films are clearly smaller than those of cold-crystallized films. Lamella of the $scCO_2$-treated films are particularly fine, close to 2 nm thick. It is believed that the $scCO_2$-treated films possess fine crystallites. However, it is not clear from Figure 9 that the fineness of the crystal structure is due to either temperature alone or the $scCO_2$-treatment effect. We focus on the surface area in the two-phase system, which involves the crystalline and amorphous phases of the $scCO_2$-treated and cold-crystallized PEN films. The specific surface area S/V is the ratio of surface area per unit volume where the crystalline and amorphous domains come in contact with each other. Here S/V is estimated from the following equation:[35]

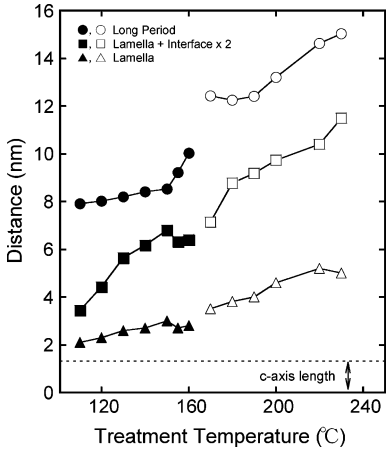

Figure 9. Relation between higher-order structure calculated by SAXS and treatment temperature in $scCO_2$-treated (closed symbols) and cold-crystallized (open symbols) PEN films.

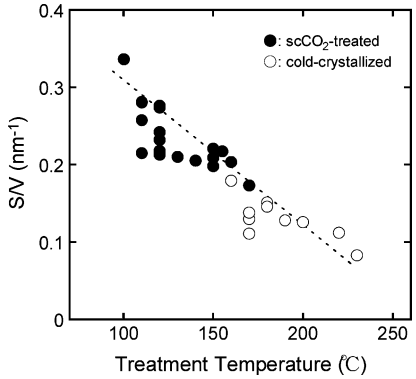

Figure 10. Specific surface area S/V vs treatment temperature of crystallized PEN films.

$$\frac{S}{V} = \frac{8\pi K_p \phi_1 \phi_2}{\int_0^\infty s\tilde{I}(s)\,\mathrm{d}s} \tag{7}$$

where K_p is the Polod constant that can be obtained from the intercept of the corrected SAXS plot ($\ln \tilde{I}(s) = -3 \ln s + \ln K_p$); ϕ_1 and ϕ_2 refer to each volume fraction. In the case of two-phase system such as crystal domains dispersed into the amorphous phase, S/V increases with decreasing the crystallite size and with increasing number of crystallites. Figure 10 shows the relation between S/V and the treatment temperature for $scCO_2$-treated and cold-crystallized PEN. Here S/V increases

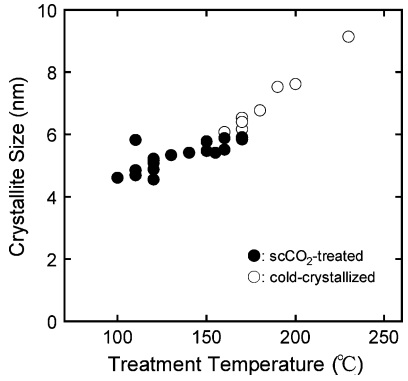

Figure 11. Crystallite size in (100) normal direction vs treatment temperature of crystallized PEN films.

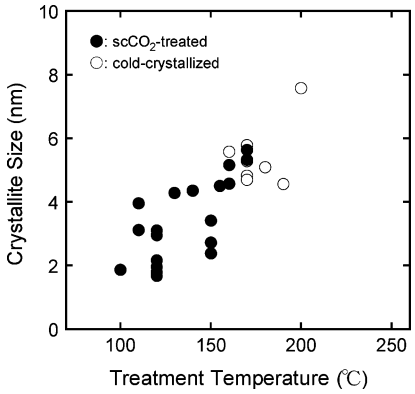

Figure 12. Crystallite size in (001) normal direction vs treatment temperature of crystallized PEN films.

with decreasing treatment temperature and was higher in the $scCO_2$-treated films than in the cold-crystallized films. The relation between S/V and the treatment temperature of both treatment films shows the same trend. The resulting fineness of crystal structure in the $scCO_2$-treated PEN films may increase with decreasing treatment temperature. We now discuss the validity of the S/V in detail using the equation

$$\frac{S}{V} = \frac{\phi_d S_d}{V_d} = \frac{3\phi_d}{r} \tag{8}$$

where ϕ_d is the volume fraction of the crystalline domain, S_d is the domain surface area ($=4\pi r^2$), V_d is the volume for one domain ($=4\pi r^3/3$), and r is the domain radius. We used the crystallinity from WAXD (0.2−0.3) for ϕ_d and the average crystallite size (4−6 nm) for r. The resulting S/V was calculated to be between 0.2 and 0.45, in relatively good agreement with the data in Figure 10.

Crystallite Size of $scCO_2$-Treated PEN. The crystallite size of $scCO_2$-treated and cold-crystallized PEN films was calculated from eq 2. Figures 11 and 12 show the relation between the crystallite size obtained from the (100) and (001) planes and the treatment temperature for $scCO_2$-treated and cold-crystallized PEN films. The crystallite size of $scCO_2$-treated films is much smaller than that of the cold-crystallized films. The (001) plane data in Figure 12 seem to vary widely because the diffraction peaks are much weaker than for the other planes. The crystallite size calculated from the (001) plane corresponding to the length along the *c*-axis is 2−8 nm, in good agreement with the lamella thickness (see Figure 9, 2−5 nm). Table 1 summarizes the long period L, lamella l_c, interface E, and amorphous thickness l_a ($l_a = L - l_c - 2E$) of the PEN film treated with $scCO_2$ at 160 °C under 20 MPa for 90 min, and the film cold-crystallized at 160 °C for 1440 min. The crystallinity calculated from eq 1 is also shown. There is little difference in the crystallinity χ_c between the cold-160 and the $scCO_2$-160 despite the large difference of the crystallization time, which shows the fast crystallization under $scCO_2$ conditions. The CO_2 causes swelling of the PEN film and expansion of the free volume, which can lead to the dramatic decrease in T_g for smooth crystallization at relatively low temperature. This table reveals that all SAXS data are almost the same values between cold-160 and the $scCO_2$-160. These indicate that the higher-order structure of PEN is strongly affected by the treatment temperature. This is probably due to the fact that the higher-order structure of semicrystalline polymer is considerably affected by the number of nuclei formed during crystallization, which has strong temperature dependence. Regarding the crystallite size and the degree of crystallinity, $scCO_2$ treatment should promote the creation of nuclei in the amorphous phase. In general, it is easier to create and increase the number of nuclei at low temperatures; therefore, the fine crystallites can be obtained from the $scCO_2$ treatment at low temperature. Here, however, it remains unclear about the role of CO_2 molecules in the formation of nucleus. Further experiments using other supercritical fluid solvents will be needed for more insight into the effect of CO_2 on the nucleation and crystallization for PEN.

Table 1. Higher-Order Structure of $scCO_2$-Treated at 20 MPa for 90 min ($scCO_2$-160) and Cold-Crystallized at 160 °C for 1440 min (cold-160)

SAXS data (nm)	$scCO_2$-160	cold-160
long period L	10.0	10.2
lamella l_c	2.8	3.1
interface E	1.8	1.8
amorphous l_a	3.6	3.6
χ_c[a] (%)	29.4	26.8

[a] Calculated from WAXD.

Conclusions

A crystalline structure PEN film was prepared using $scCO_2$ treatment at an abnormal temperature range, from 110 to 170 °C. After the treatment, the T_g of PEN films was reduced by more than 50 °C and the films were crystallized. The change in the absorbance intensity at 2335 cm^{-1} (C═O) obtained from FT-IR measurement was consistent with the change in T_g and T_c. The linear relation between T_g and the absorbance intensity shows that sorption of CO_2 molecules into the film is responsible for the fall in T_g. The T_g under CO_2 exposure conditions was estimated according to desorption kinetics. Moreover, an increase in the treatment pressure raised the amount of absorbed CO_2 and reduced T_g, promoting the crystallization. The higher-order structure, long period, lamella, and interface thickness of the crystallized PEN films were calculated from the SAXS profile and one-dimensional correlation function. It was clear that all these parameters are linearly related to the treatment temperature. The crystallite size obtained from the Scherrer equation decreased with decreasing treatment temperature. It appears that the higher-order structure can be decided only from the treatment temperature; the $scCO_2$ treatment may promote the creation of nuclei in the amorphous phase at low

temperatures, following the formation of fine crystallites and fine higher-order structure.

Acknowledgment. This study has been partially supported by The 21st Century Center of Excellence (COE) program from the Japanese Ministry of Education, Culture, Sports, Science and Technology; "Creation of Molecular Diversity and Development of Functionalities" at Tokyo Institute of Technology.

References and Notes

(1) Cheng, S. Z. D.; Wunderlich, B. *Macromolecules* **1988**, *21*, 789−797.
(2) Buchner, S.; Wiswe, D.; Zachmann, H. G. *Polymer* **1989**, *30*, 480−488.
(3) Chen, D.; Zachmann, H. G. *Polymer* **1991**, *32*, 1612−1621.
(4) Liu, J.; Sidoti, G.; Hommema, J. A.; Geil, P. H.; Kim, J. C.; Cakmak, M. J. *Macromol. Sci. Phys.* **1998**, *B37*, 567−586.
(5) Vasanthan, N.; Salem, D. R. *Macromolecules* **1999**, *32*, 6319−6325.
(6) Kampert, W. G.; Sauer, B. B. *Polymer* **2001**, *42*, 8703−8714.
(7) Murakami, S.; Mishikawa, Y.; Tsuji, M.; Kawaguchi, A.; Kohjiya, S.; Cakmak, M. *Polymer* **1995**, *36*, 291−297.
(8) Murakami, S.; Yamakawa, M.; Tsuji, M.; Kohjiya, S. *Polymer* **1996**, *37*, 3945−3951.
(9) Garcia Gutierrez, M. C.; Karger-Kocsis, J.; Riekel, C. *Macromolecules* **2002**, *35*, 7320−7325.
(10) Garcia Gutierrez, M. C.; Rueda, D. R.; Calleja, F. J. B.; Stribeck, N.; Bayer, R. K. *J. Mater. Sci.* **2001**, *36*, 5739−5746.
(11) Li, L.; Wang, C.; Huang, R.; Zhang, L.; Hong, S. *Polymer* **2001**, *42*, 8867−8872.
(12) Garcia Gutierrez, M. C.; Rueda, D. R.; Calleja, F. J. B.; Stribeck, N.; Bayer, R. K. *Polymer* **2003**, *44*, 451−455.
(13) Kim, S. J.; Nam, J. Y.; Lee, Y.-M.; Im, S. S. *Polymer* **1999**, *40*, 5623−5629.
(14) Okamoto, M.; Kubo, H.; Kotaka, T. *Macromolecules* **1998**, *31*, 4223−4231.
(15) Yoon, W. J.; Myung, H. S.; Kim, B. C.; Im, S. S. *Polymer* **2000**, *41*, 4933−4942.
(16) McHugh, M. A.; Krukonis, V. J. *Supercritical Fluid Extraction: Principles and Practice*, 2nd ed; Butterworth Publishers: Stoneham, MA, 1994.
(17) Sun, Y.-P. *Supercritical Fluid Technology in Materials Science and Engineering*; Marcel Dekker: New York, 2002.
(18) Cooper, A. I. *J. Mater. Chem.* **2000**, *10*, 207−234.
(19) Kendall, J. L.; Canelas, D. A.; Young, J. L.; DeSimone, J. M. *Chem. Rev.* **1999**, *99*, 543−563.
(20) Handa, Y. P.; Capowski, S.; O'Neill, M. *Thermochim. Acta* **1993**, *226*, 177−185.
(21) Shieh, Y.-T.; Su, J.-H.; Manivannan, G.; Lee, P. H. C.; Sawan, S. P.; Spall, W. D. *J. Appl. Polym. Sci.* **1996**, *59*, 695−705.
(22) Handa, Y. P.; Zhang, Z. *Macromolecules* **1997**, *30*, 8505−8507.
(23) Chiou, J. S.; Barlow, J. W.; Paul, D. R. *J. Appl. Polym. Sci.* **1985**, *30*, 3911−3924.
(24) Mizoguchi, K.; Hirose, T.; Naito, Y.; Kamiya, Y. *Polymer* **1987**, *28*, 1298−1302.
(25) Fleming, G. K.; Koros, W. J. *Macromolecules* **1986**, *19*, 2285−2291.
(26) Schultze, T. D.; Engelmann, I. A. D.; Boehning, M.; Springer, J. *Polym. Adv. Technol.* **1991**, *2*, 123−126.
(27) Handa, Y. P.; Roovers, J.; Wang, F. *Macromolecules* **1994**, *27*, 5511−5516.
(28) Zhang, Z.; Handa, Y. P. *J. Polym. Sci., Part B: Polym Phys.* **1998**, *36*, 977−982.
(29) Condo, P. D.; Paul, D. R.; Johnston, K. P. *Macromolecules* **1994**, *27*, 365−371.
(30) Kishimoto, Y.; Ishii, R. *Polymer* **2000**, *41*, 3483−3485.
(31) Kazarian, S. G.; Vincent, M. F.; Bright, F. V.; Liotta, C. L.; Eckert, C. A. *J. Am. Chem. Soc.* **1996**, *118*, 1729−1736.
(32) Flichy, N. M. B.; Kazarian, S. G.; Lawrence, C. J.; Briscoe, B. J. *J. Phys. Chem. B* **2002**, *106*, 754−759.
(33) Calleja, F. J. B.; Vonk, C. G. *X-ray Scattering of Synthetic Polymers*; Elsevier: New York, 1989.
(34) Ruland, W. *J. Appl. Crystallogr.* **1971**, *4*, 70−73.
(35) Koberstein, J. T.; Morra, B.; Stein, R. S. *J. Appl. Crystallogr.* **1980**, *13*, 34−45.

MA050373Q